Electronic Absorption Spectra of Neutral Pentacene ($C_{22}H_{14}$) and Its Positive and Negative Ions in Ne, Ar, and Kr Matrices

Thomas M. Halasinski, Douglas M. Hudgins, Farid Salama,* and Louis J. Allamandola

NASA Ames Research Center, Mail Stop: 245-6, Moffett Field, California 94035-1000

Thomas Bally

Institute of Physical Chemistry, University of Fribourg, Pérolles, CH-1700 Fribourg, Switzerland

Received: March 28, 2000; In Final Form: June 5, 2000

The absorption spectra of neutral pentacene ($C_{22}H_{14}$) and its radical cation ($C_{22}H_{14}^+$) and anion ($C_{22}H_{14}^-$) isolated in solid Ne, Ar, and Kr have been measured from the ultraviolet to the near-infrared. The associated vibronic band systems and their spectroscopic assignments are discussed together with the physical and chemical conditions governing molecular anion production in matrices doped with alkali metal (Na or K). TD-DFT calculations were carried out to assist in the assignments for the measured spectral features of the pentacene ions.

1. Introduction

While it has proved difficult to unambiguously identify individual molecular species responsible for a distinctive family of infrared emission features observed from matter at all stages of the lifecycle of the interstellar medium (ISM), there is now strong evidence that these ubiquitous emission features arise from carbonaceous aromatic materials and, in particular, from neutral and positively charged polycyclic aromatic hydrocarbons (PAHs).[1] PAHs are also thought to contribute to the diffuse interstellar bands (DIBs) seen in absorption in the optical spectra of stars that are obscured by diffuse interstellar clouds.[2]

Negatively charged PAHs are also expected to play an important role in the evolution of interstellar clouds.[2a,3] Although anionic PAHs may be an important component in the interstellar medium, the spectroscopy of negatively charged PAHs in an astrophysically relevant environment has been largely unexplored. Electronic spectra of several PAH anions have been previously studied in glassy organic solids.[4] This environment induces strong perturbations on the energy levels of the trapped ions, making comparisons to astronomical data difficult, if not impossible. Matrix-isolation spectroscopy, however, is the dominant method for the study of isolated ions and is an especially well-suited technique for the simulation of the low temperature and low molecular density interstellar environments.[5] An extensive survey of the electronic spectroscopy of PAH ions in rare gas matrices has shown that, with the exception of pentacene isolated in Ar matrices,[6] no spectroscopic signatures associated with PAH anions have been reported thus far. The relatively high electron affinity of pentacene (1.35 eV)[7] may explain the observation of spectral features of the pentacene anion in an Ar matrix.[6,8]

A particularly successful method of producing molecular anions in rare gas matrices has been developed by Kasai[9] for electron spin resonance spectroscopy studies. In this method, Na atoms are used as matrix dopants. Upon irradiation with suitable light, the metal atoms act as electron donors, which leads to the formation of isolated molecular guest anions. This report describes experimental studies in which we have co-deposited the PAH pentacene ($C_{22}H_{14}$) with an alkali metal (Na or K) in Ne, Ar, and Kr matrices, photoionized the alkali metal trapped in the matrix, and probed the matrices spectroscopically from the ultraviolet (180 nm) to the infrared (500 cm^{-1}). Given its relatively high electron affinity and the availability of spectroscopic data on its anion, pentacene represents the ideal prototype to explore and optimize the use of alkali metal dopants in rare gas matrices to facilitate the production of matrix-isolated PAH anions while prohibiting the formation of PAH counterions within the matrix. The information gained from these experiments can be used to assist in the spectral assignment process when PAH ions and PAH counterions are simultaneously formed in matrix-isolation experiments.

2. Experimental Section

The experimental instrumentation used in the matrix-isolation studies reported here has been previously described in detail. Two independent instruments were employed in these studies, a UV/visible/near-IR spectrometer[10] and an FTIR spectrometer,[11] each equipped with its own dedicated sample vacuum chamber and matrix deposition source. A brief review will be given here of the procedures followed in preparation of the sample matrix, along with a more detailed description of the modifications used to co-deposit alkali metal vapor along with pentacene vapor and the lamps used during photoionization of the matrices.

The UV/visible/near-IR instrument is equipped with a sapphire sample window cooled to 4.2 K by an extended liquid helium transfer cryostat, while the FTIR instrument uses a CsI window cooled to 10 K by a closed-cycle helium refrigerator. Both sample windows can be rotated under vacuum to face, alternatively, two spectroscopic window ports, the matrix gas and PAH/alkali metal vaporization lines, and a MgF_2 vacuum-UV window port. Single-beam spectra of the cold substrate were collected before the matrix was deposited and used as the background for all spectra reported unless noted otherwise.

The vaporization and co-deposition of pentacene and the alkali metals was performed using Pyrex tubes (12.7 mm OD)

* Corresponding author. E-mail: fsalama@mail.arc.nasa.gov.

10.1021/jp0011544 CCC: $19.00
Published on Web 07/19/2000

mounted on the sample chamber and externally heated with heating tape. The tubes were positioned between 4 and 5 cm from the cold window. The temperature of each tube was monitored using a chromel/alumel thermocouple mounted on the exterior of each tube with Al foil tape. Some experiments reported here also utilized two resistively heated stainless steel tubes (5 mm diameter) to vaporize the pentacene and alkali metal samples.[9] These tubes were positioned 3 cm from the surface of the cold substrate. Both deposition systems produced matrices of similar spectral quality.

Matrix gas was admitted through a port at a position 45° from the plane of the substrate surface and the median between the tubes containing pentacene and alkali metal. Typical deposition temperatures for pentacene, Na, and K were 175−225, 205−235, and 110−130 °C, respectively. Ne flow rates were estimated to be 12 mmol/h while typical Ar flow rates were decreased to 0.5 mmol/h to reduce the light scattering of the matrix. Based on these flow rates and vaporization temperatures, the matrix/pentacene/alkali metal ratio is estimated to be in excess of 800/1/1. Typical deposition times varied from 2 to 4 h.

Three photolysis lamps were used. An OSRAM mercury arc lamp (HBO 100 W/2) produced radiation from 300 to 1200 nm (4.1−1.0 eV) with the maximum intensity at 2.1 eV. A microwave-powered, hydrogen flow (10% H_2/He), discharge lamp (Opthos Instruments MPG 4M) produced nearly monochromatic radiation in the Lyman α line at 121.6 nm (10.2 eV). Experiments were also performed in which a standard Na arc lamp [589 nm (2.1 eV)] was used as a photolysis source. Typical photolysis times ranged from 2 to 20 min.

Pentacene (98+%) was obtained from Aldrich Chemical Co. and was used as received. Na chunks (98%) stored in mineral oil were obtained from Aldrich Chemical Co. Immediately prior to use, Na pieces (~3 mm^3) were prepared by cleaving larger chunks to produce essentially clean and oil-free Na samples. K samples were prepared in a similar fashion. Ne (Cryogenic Rare Gas 99.9995%), Ar (Matheson 99.998%), and Kr (Cryogenic Rare Gas 99.995%) research grade rare gases were used without further purification.

All geometry optimizations and frequency calculations were carried out with the B3LYP density functional method[12,13] using the 6-31G* basis set. Vertical and adiabatic excited-state energies were evaluated either as B3LYP energy differences or by the recently introduced time-dependent density functional theory (TD-DFT), as described by Stratmann et al.,[14] which also permits the calculation of electronic transition moments. All DFT calculations were carried out with the Gaussian 98 program.[15] As a crosscheck we also performed excited-state calculations by the semiempirical INDO/S method[16] as implemented in the ZINDO program.[17]

3. Results and Discussion

A series of studies were performed to ascertain the feasibility of (i) producing PAH anions from neutral PAH precursors isolated in rare gas matrices doped with alkali metals and (ii) to measure their electronic absorption spectra without substantially decreasing the abundance of PAH anions through electron photodetachment. The ultimate objective is to obtain the spectra of molecular ions in Ne matrices to permit the measurement of electronic transitions with minimal perturbations. We report and discuss the spectra which illustrate the successful production of isolated pentacene anions in Ne matrices and the optimal conditions for their production without the concurrent production of molecular cations. We also report and discuss the assignment of the electronic spectra of the pentacene cations as well as the theoretical calculations used to support these assignments.

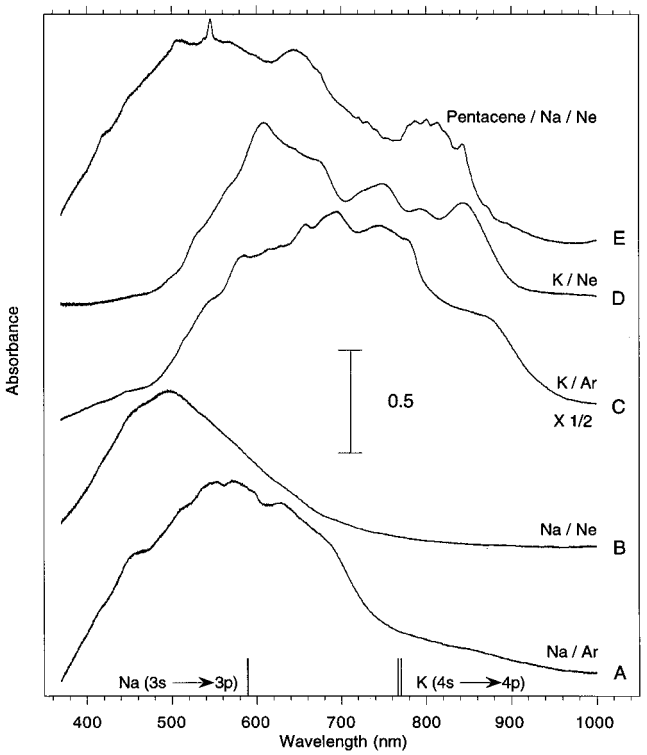

Figure 1. The visible/near-IR spectra of a co-deposit of (A) Na in Ar; (B) Na in Ne; (C) K in Ar; (D) K in Ne; and (E) pentacene and Na in Ne. Note that the spectrum displayed in (E) corresponds to a 4 h deposition while the others were taken from 2 h depositions. The gas-phase spectral positions of the D lines of Na and K are displayed as vertical lines on the bottom of the plot. The doublet D lines of Na are not resolved with the scale used for this plot.

3.1. Electronic Spectroscopy of the Alkali Metals, Na, and K, Isolated in Rare Gas Matrices. Initial experiments focused on the spectra of isolated alkali metals (Na and K) in both Ar and Ne matrices to assist in the assignment of new spectral features observed when the alkali metals were co-deposited with pentacene in a rare gas matrix. Figure 1A,B display the visible/near-IR spectra (370−1000 nm) obtained when Na is deposited in Ar and Ne matrices, respectively. Figure 1C,D display the same spectral region when K is deposited in Ar and Ne, respectively. In both cases, no absorbance features are observed in the UV range up to the detection limit of the spectrometer (180 nm). The spectral structure is highly sensitive to experimental parameters such as the vaporization temperature of the alkali metal, the flow rate of the rare gas, and the temperature of the matrix. These observations are in global agreement with previous studies[18−20] which show that alkali metals produce a number of broad bands in the visible/near-IR when trapped in rare gas matrices.

3.2. Electronic Spectroscopy of Pentacene Isolated in Rare Gas Matrices. The electronic spectrum of neutral pentacene isolated in rare gas matrices (Ne, Ar, and Kr) exhibits 3 band systems in the 250−1000 nm spectral window (Figure 2) associated with transitions to the (1^1B_{2u}), (1^1B_{3u}), and (2^1B_{3u}) states.[21] The positions of the bands are listed in Table 1. To our knowledge, high-resolution, gas-phase measurements of neutral pentacene have been reported only for the first excited electronic state band origin at 536.2 nm.[22] This compares well with our measurement in a Ne matrix at 542.7 nm. The gas-phase to matrix fractional shift ($\nu_{(gas-matrix)}/\nu_{gas}$) for this band

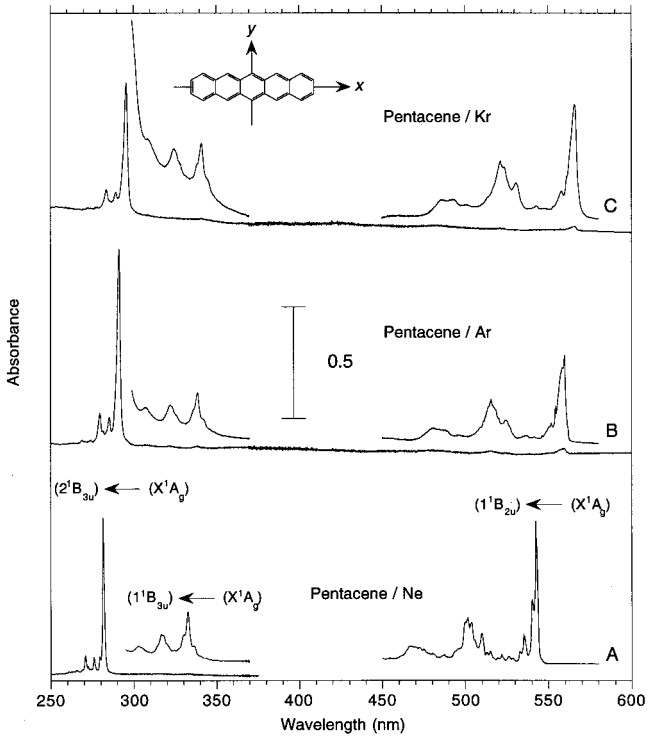

Figure 2. The UV/visible spectra of a co-deposit of (A) pentacene in Ne; (B) pentacene in Ar; and (C) pentacene in Kr. Spectra showing the 2^1B_{3u} transition were taken after 5 min depositions. Spectra showing the 1^1B_{3u} and 1^1B_{2u} transitions were taken after 2 h depositions to enhance the weaker spectral features.

origin corresponds to 1.2%, 4.2%, and 5.3%, respectively in Ne, Ar, and Kr. The increase in the matrix-induced shift indicates an enhanced interaction between the trapped pentacene molecule and the host matrix as is expected from the increasing polarizability of the matrix material when going from Ne to Kr. The influence of the molecular size of the trapped molecule on the matrix shift can be seen by comparing the fractional shift of 1.2% for pentacene in Ne observed here to the 0.25% shift reported for naphthalene in Ne.[10a] As in naphthalene (also of D_{2h} symmetry), the totally symmetric vibrational modes are expected to dominate the vibronic transitions of pentacene.[10a] Using the experimental Raman band positions of pentacene[23] as a guide, we have made tentative assignments for most of the observed vibronic transitions (see Table 1).

3.3. Electronic and vibrational spectroscopy of pentacene isolated in alkali-metal doped rare gas matrices. Figure 1E displays the visible/near-IR absorption spectrum obtained after Na and pentacene are co-deposited in a Ne matrix for 4 h. Most of the broad underlying absorption observed in this spectrum corresponds to that observed when only Na is deposited in Ne (see the 2 h deposition displayed in Figure 1B). Absorption bands due to the transitions associated with the $(X^1A_g) \rightarrow (1^1B_{2u})$ band system of isolated neutral pentacene (Figure 2 and Table 1) are also observed. Additional spectral features are observed in the region between 620 and 870 nm which only appear when *both* pentacene and Na are present in the matrix. Co-deposition of K with pentacene in rare gas matrices also reveals new bands in the visible/near-IR which are not present when each of the species is trapped individually in the matrix.

Experiments in which the deposition temperature of pentacene and the alkali metal were varied produced changes in the relative band strengths in the infrared, clearly indicating that complexes involving pentacene molecule(s) and alkali metal atoms were formed *during* the matrix deposition. In the remaining discussion, we will refer to these uncharacterized species as alkali metal−pentacene complexes. Evidence is found for the simultaneous presence of isolated pentacene, isolated alkali metal atoms, alkali metal dimers, as well as alkali metal−pentacene complexes. Similar observations of the concurrent production of anions in matrices in both isolated sites and in sites where there is significant interaction with the alkali metal cation have been previously reported.[24] We discuss below the pre- and post-photolysis spectra of pentacene isolated in alkali atom-doped matrices.

3.3.1. Pentacene Isolated in a Na-Doped Ar Matrix. Pre-photolysis. The mid-IR spectra of co-deposits of alkali metal and pentacene in Ar matrices were also measured and compared to the previous measurements of pentacene isolated in Ar.[6,8,25] Figure 3A displays the mid-IR spectrum (1450−1290 cm^{-1}) of a co-deposit of Na and pentacene in solid Ar. This region has been selected from the entire spectral region scanned (5000−500 cm^{-1}) because it shows the most intense vibrational transitions of the pentacene anion[6,8] and alkali metal−pentacene complexes.

Comparison of Figure 3A to Figure 3E indicates the presence of isolated neutral pentacene in the co-deposit of alkali metal and pentacene through the vibrational band observed at 1298.9 cm^{-1} (note the change in scale between Figure 3A and 3E). The full absorbance of the most intense features in Figure 3A, however, cannot be due to isolated neutral pentacene. The band observed at 1372.6 cm^{-1} happens to fall at the same position as that previously assigned to the most intense infrared band of the pentacene anion.[6,8] Since the second most intense infrared band of the anion at 1349.2 cm^{-1} is not detected, or is significantly weaker than expected, the full absorbance of the band at 1372.6 cm^{-1} cannot be due to the isolated pentacene anion.

The absence of the pentacene anion in the matrix is further confirmed by the near-IR spectrum of the same sample which is shown Figure 4A. The band at 882.2 nm, assigned to the pentacene anion by Szczepanski et al.,[6] is not observed in this spectrum. All features in this spectrum are thus assigned to Na−pentacene complexes, as they only appear when both species are present within the matrix, similar to the spectral features in Figure 3A. On the basis of the absence of the stronger pentacene anion bands in the near-IR shown in Figure 4A and the absence of the second strongest mid-IR anion band discussed above, it is concluded that the vibrational band measured at 1372.6 cm^{-1} in Figure 3A is not due to the isolated pentacene anion but rather to a Na−pentacene complex.

Post-photolysis. The spectrum of the same sample that was used to produce Figure 4A following 4 min of photolysis with the high-pressure mercury arc lamp is shown in Figure 4B. The most notable change is the appearance of 3 new, strong bands at 882.1, 889.0, and 908.1 nm along with some weaker features (see Table 2). The position of the 882.1 nm band matches well that previously assigned to the pentacene anion in Ar at 882.2 nm.[6] We note that the spectral features below 850 nm, and assigned to Na−pentacene complexes, are largely unaffected by the photolysis (compare Figures 4A,B).

The post-photolysis mid-IR spectrum of the sample used to produce Figure 4B is reproduced in Figure 3B. The most notable new band appears at 1349.2 cm^{-1}. The most intense band at 1321.1 cm^{-1} changes only slightly, while that at 1372.6 cm^{-1} grows by ∼30%. The difference spectrum displayed in Figure 3C shows that the two bands expected for the pentacene anion in this region of the spectrum do indeed grow in intensity with the expected ratio from that of the published spectrum of the

TABLE 1: Vibronic Transitions of Neutral Pentacene Isolated in Ne, Ar, and Kr Matrices Shown in Figure 2[a]

	Ne			Ar			rel. shift	Kr			rel. shift
assignment	λ (nm)	ν (cm^{-1})	$\Delta\nu$ (cm^{-1})	λ (nm)[c]	ν (cm^{-1})	$\Delta\nu$ (cm^{-1})	$\Delta\nu_{(Ne-Ar)}/\nu_{Ne}$ (%)	λ (nm)	ν (cm^{-1})	$\Delta\nu$ (cm^{-1})	$\Delta\nu_{(Ne-Kr)}/\nu_{Ne}$ (%)
υ_{CC} stretch	270.7	36 941	1417	279.6	35 765	1425	3.2	283.6	35 261	1420	4.5
υ_{CH} ∥ bend	275.8	36 258	734	285.2	35 063	722	3.3	289.4	34 554	713	4.7
$2^1B_{3u} \leftarrow X^1A_g$	281.5[b]	35 524	0	291.2[b]	34 341	0	3.3	295.5[b]	33 841	0	4.7
υ_{CH} stretch	303.0	33 003	2928	307.0	32 573	3022	1.3	308.9	32 373	3047	1.9
υ_{CC} stretch	316.5	31 596	1520	322.1	31 046	1495	1.7	324.4	30 826	1501	2.4
$1^1B_{3u} \leftarrow X^1A_g$	332.5[b]	30 075	0	338.4[b]	29 551	0	1.7	341.0[b]	29 326	0	2.5
$2\upsilon_{CC}$ stretch	466.9	21 418	2991	481.2	20 781	2918	3.0	487.0	20 534	2866	4.1
				(480.2)	(20 825)						
	472.6	21 160	2733	488.2	20 483	2620	3.2	492.8	20 292	2624	4.1
υ_{CC} stretch	501.5	19 940	1514	515.7	19 391	1528	2.8	521.4	19 179	1511	3.8
				(515.6)	(19 395)						
υ_{CH} ⊥ bend	510.0	19 608	1181	524.7	19 059	1195	2.8	530.8	18 839	1172	3.9
υ_{CCC} ∥ bend	535.2	18 685	258	551.8	18 123	259	3.0	558.0	17 921	253	4.1
	540.2	18 512	85	554.4	18 038	174	2.6	561.3	17 816	148	3.8
$1^1B_{2u} \leftarrow X^1A_g$	542.7[b]	18 426	0	559.8[b]	17 864	0	3.1	566.0[b]	17 668	0	4.1
				(559.7)	(17 867)						

[a] The axis system adopted here is the following: *x*, long axis; *y*, short axis; and *z* , out-of-plane axis. [b] Strongest band of the system. [c] Values in parentheses are taken from ref 6.

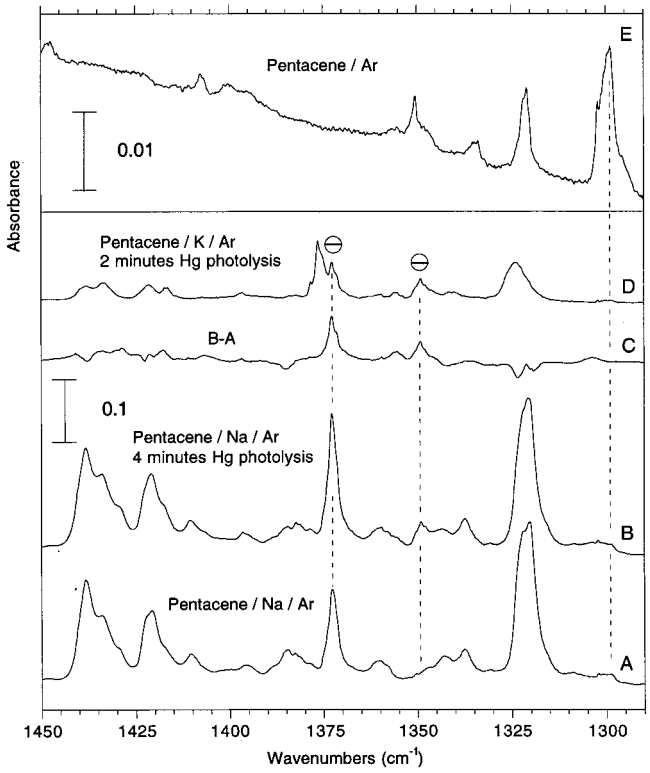

Figure 3. The mid-IR spectra of (A) a 2 h deposit of Na and pentacene in Ar; (B) the same sample after 4 min of high-pressure mercury lamp photolysis; (C) the difference spectrum of (B) and (A); (D) a 2 h deposit of K and pentacene in Ar followed by 2 min of mercury arc lamp photolysis; and (E) a 3 h deposit of pentacene in Ar. Note the expanded scale used in Figure 3E.

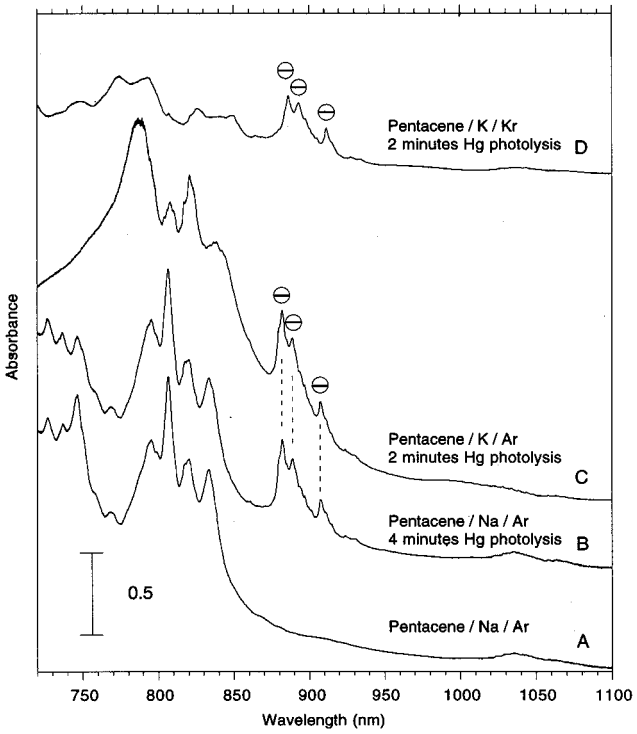

Figure 4. The near-IR spectra of (A) a 2 h deposit of Na and pentacene in Ar; (B) the same sample after 4 min of high-pressure mercury lamp photolysis; (C) a 2 h deposit of K and pentacene in Ar followed by 2 min of mercury arc lamp photolysis; and (D) a 2 h deposit of K and pentacene in Kr followed by 2 min of mercury arc lamp photolysis.

pentacene anion in Ar.[8] The intensity ratio between 1372.6 and 1349.2 cm^{-1} in Figure 3B is not commensurate with that in the published spectrum due to the overlap of two bands in the region of the 1372.6 cm^{-1} feature. One is due to the isolated pentacene anion while the other is due to a Na−pentacene complex. This conclusion is further verified by replacing the electron donor (Na) by K as described in the next paragraph.

3.3.2. Pentacene Isolated in K-Doped Ar and Kr Matrices. While the position of the most intense near-IR band at 882.1 nm obtained on photolysis of the pentacene/Na-doped Ar matrix indicates the presence of pentacene anions, the presence of strong spectral features in the mid- and near-IR due to the formation of complexes between the Na and pentacene raises the question whether the anion is truly isolated within the matrix, or whether it is in contact with one or more alkali metals situated in the vicinity. To investigate the nature of the mid- and near-IR absorptions and the degree of isolation of the anion, similar experiments were performed in which K was used in place of Na.

Figure 3D displays the mid-IR spectrum of an Ar matrix containing K and pentacene after 2 min of photolysis by a high-pressure mercury lamp. The most notable result of replacing Na by K is the appearance of a doublet at 1376.4 and 1372.6 cm^{-1}. The positions and intensities of the 1372.6 and the 1349.2

TABLE 2: Vibronic Transitions of the Pentacene Anion Isolated in Ne, Ar, and Kr Matrices Shown in Figures 4 and 5[a]

	Ne			Ar			rel. shift	Kr			rel. shift
assignment	λ (nm)	ν (cm^{-1})	$\Delta\nu$ (cm^{-1})	λ (nm)[c]	ν (cm^{-1})	$\Delta\nu$ (cm^{-1})	$\Delta\nu_{(Ne-Ar)}/\nu_{Ne}$ (%)	λ (nm)	ν (cm^{-1})	$\Delta\nu$ (cm^{-1})	$\Delta\nu_{(Ne-Kr)}/\nu_{Ne}$ (%)
$1^2B_{2g} \leftarrow X^2B_{1u}$	872.6[b]	11 460	0	882.1[b] (882.2)	11 337 (11 335)	0	1.1	886.4[b]	11 282	0	1.6
a_g (1^2B_{3g})	883.8	11 315	253	889.0	11 249	237	0.6	893.1	11 197	227	1.0
$1^2B_{3g} \leftarrow X^2B_{1u}$	904.0[b]	11 062	0	908.1[b]	11 012	0	0.5	911.6[b]	10 970	0	0.8

[a] The axis system adopted here is: *x*, long axis; *y*, short axis; and *z* is the out of plane axis. [b] Strongest band of the system. [c] Values in parentheses are taken from ref 6.

cm^{-1} bands are similar to those reported earlier for the isolated pentacene anion and to those observed in Figure 3C.[8] The band at 1376.4 cm^{-1} in Figure 3D is therefore assigned to a complex between K and pentacene and is likely due to a vibrational mode similar to that which contributed intensity to the band at 1372.6 cm^{-1} in Figure 3B.

The mid-IR bands assigned to the *isolated* pentacene anion do not display a measurable shift when replacing Na by K in the matrix. The electronic spectrum of the anion may, however, be regarded as a more sensitive measure of the degree of interaction between the alkali metal and the pentacene molecule within the matrix. Figure 4C shows the near-IR spectrum of the same photoionized sample used to produce the spectrum in Figure 3D. While the spectral features below 850 nm in Figure 4C have strongly changed in appearance from those observed in Figure 4B, as one would expect for complexes formed between the pentacene molecule and different alkali metals within the matrix, the three intense bands assigned to the pentacene anion do not change in position nor in shape. On the basis of these observations, we conclude that the pentacene anions which produce bands in the 882−912 nm region are indeed isolated from the alkali metal electron donors within the matrix.

Figure 4D shows the near-IR spectrum of a deposit of K and pentacene in Kr followed by 2 min of photolysis by the high-pressure mercury lamp. The experimental parameters used to obtain this spectrum were the same as those used to obtain Figure 4C except that the temperature used to vaporize K was lowered from 130 to 113 °C. As expected from the more polarizable Kr atoms, the bands of the pentacene anion in Kr have shifted slightly toward the red as compared to the anion in Ar (see Table 2). Comparison of the spectral features attributable to the K− pentacene complex in Kr to those observed in Ar in Figure 4C suggests that the formation of the alkali metal−pentacene complex is, as expected, strongly matrix dependent.

3.3.3. Pentacene Isolated in a Na-Doped Ne Matrix. The experiments discussed thus far have examined the feasibility of producing and detecting isolated pentacene anions within a rare gas matrix. The primary objective here is, however, to measure the electronic spectrum of the pentacene ion in the least perturbing environment (i.e., isolated in a Ne matrix). Of additional interest to us is the study of the effect of increasing the energy of the probing radiation on the photodetachment of the electron from the anion (i.e., on the yield of pentacene anions) as detected through their strongest electronic absorption transitions.

Figure 5A displays the near-IR spectrum of a pentacene:Na:Ne matrix photoionized with the 2.1 eV output of a Na lamp. This radiation is sufficient to photoionize Na within the matrix.[9] The bands at 872.6, 883.8, and 904.0 nm, which are reported here for the first time, are assigned to the isolated pentacene anion in Ne (see Table 2). Since the gas-phase ionization energy

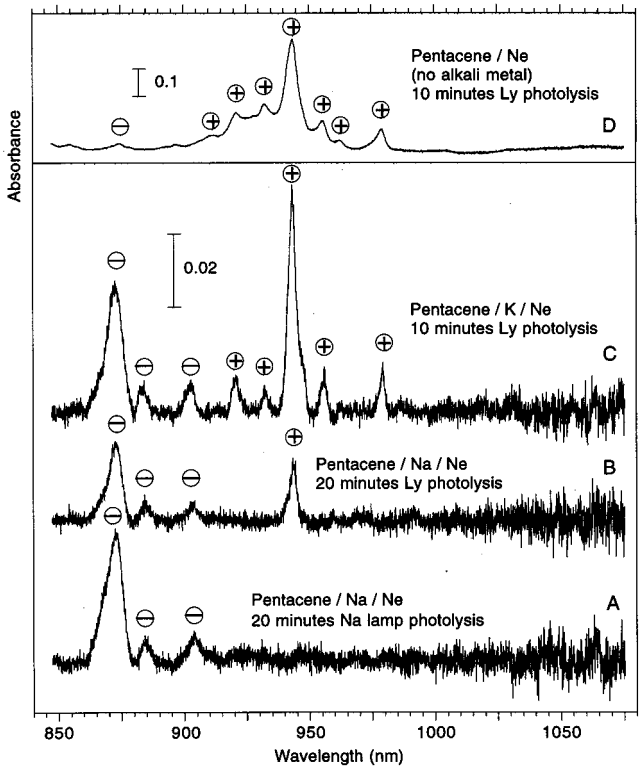

Figure 5. The near-IR spectra of (A) a 2 h deposit of Na and pentacene in Ne followed by 20 min of Na lamp photolysis; (B) the same sample after an additional 20 min of Lyman α photolysis; (C) a 2 h deposit of K and pentacene in Ne followed by 10 min of Lyman α photolysis; and (D) a 2 h deposit of pentacene in Ne followed by 10 min of Lyman α photolysis. The pre-photolysis spectrum in each case was used as the background for the resulting spectrum. The spectra shown in (A), (B), and (C) were baseline corrected to remove the broad underlying absorption due to the alkali metal and the alkali metal−pentacene complex shown in Figure 1E.

of pentacene[26] is 6.61 eV, pentacene cations are not produced here. When the same sample was exposed to the output of a hydrogen lamp (10.2 eV), the strongest band of the pentacene cation appeared (see Figure 5B and Table 3). The spectrum of the pentacene cation isolated in Ne (in the absence of alkali metal) following irradiation with the Lyman α line (10.2 eV) is also shown in Figure 5D for reference. The spectral features of the pentacene anion decrease slightly, but do not disappear entirely. Presumably, a dynamic equilibrium exists between the formation of pentacene anions and the photodetachment of the electrons from pentacene anions that have already formed. Thus, both the Lyman α radiation and the light used to spectroscopically probe the sample to produce Figure 4B have likely neutralized a significant portion of the anions present before photolysis. The 10.2 eV radiation, however, simultaneously produces additional anions through the process of photodetachment of electrons from neutral pentacene molecules and Na atoms in the matrix.

TABLE 3: Vibronic Transitions of the Pentacene Cation Isolated in Ne, Ar, and Kr Matrices[a]

	Ne			Ar			rel. shift	Kr			rel. shift
assignment	λ (nm)	ν (cm^{-1})	$\Delta\nu$ (cm^{-1})	λ (nm)[c]	ν (cm^{-1})	$\Delta\nu$ (cm^{-1})	$\Delta\nu_{(Ne-Ar)}/\nu_{Ne}$ (%)	λ (nm)	ν (cm^{-1})	$\Delta\nu$ (cm^{-1})	$\Delta\nu_{(Ne-Kr)}/\nu_{Ne}$ (%)
$2^2A_u \leftarrow X^2B_{3g}$	420.5[b]	23 781	0	425.1[b]	23 524	0	1.1				
				(426.0)	(23 474)						
υ_{cc} (1^2A_u)	832.1	12 018	1424	842.3	11 872	1401	1.2	845.9	11 822	1394	1.6
				(842.2)	(11 874)						
$3a_g$ (1^2B_{1u})	912.1	10 964	752	931.6	10 734	586	2.1	935.4	10 691	569	2.5
				(931.7)	(10 733)						
a_g (1^2A_u)	921.5	10 852	258	938.9	10 651	180	1.9	942.1	10 615	187	2.2
				(940.3)	(10 635)						
$2a_g$ (1^2B_{1u})	933.6	10 711	500	947.4	10 555	407	1.5	952.6	10 498	376	2.0
				(947.8)	(10 551)						
$1^2A_u \leftarrow X^2B_{3g}$	943.9[b]	10 594	0	955.0[b]	10 471	0	1.2	959.0[b]	10 428	0	1.6
				(954.1)	(10 481)						
a_g (1^2B_{1u})	955.7	10 464	252	962.1	10 394	246	0.7	965.5	10 357	236	1.0
				(961.9)	(10 396)						
	962.8	10 386	175	968.6	10 324	176	0.6	969.8	10 311	190	0.7
				(968.5)	(10 325)						
$1^2B_{1u} \leftarrow X^2B_{3g}$	979.3[b]	10 211	0	985.4[b]	10 148	0	0.6	988.0[b]	10 121	0	0.9
				(984.9)	(10 153)						
matrix site				990.3	10 098						
				(990.6)	(10 095)						

[a] The axis system adopted here is the following: *x*, long axis; *y*, short axis; and *z*, out-of-plane axis. [b] Strongest band of the system. [c] Values in parentheses are taken from ref 6.

3.*3.4. Pentacene Isolated in a K-Doped Ne Matrix.* Figure 5C shows the spectrum resulting after photoionizing a Ne matrix doped with pentacene and K with Lyman α radiation. As in the case of the sample whose spectrum is displayed in Figure 5B, spectroscopic features due to both pentacene anions and pentacene cations are observed. The position and band shape of all the features are not modified by changing the electron donor from Na to K. Just as in the comparison of Figure 4B,C discussed above, the total resemblance of the ionic features in Figure B,C allows us to conclude that the pentacene anions and cations detected in these spectra are isolated from their counterions within the matrix.

3.4. Assignments of the Vibronic Features Observed for the Pentacene Cation and Anion. The only previous assignment of the electronic absorption spectrum of the pentacene cation is that reported by Szczepanski et al.[6] In their Ar matrix study, two excited states of the cation were observed at 954.1 and 426.0 nm and assigned on the basis of the photoelectron (PE) spectrum of pentacene.[26] The first four lowest energy features observed at 990.6, 984.9, 968.5, and 961.9 nm (Table 3) were not discussed. As listed in Table 3, the spectral features of the pentacene cation isolated in Ar observed in this study are in good agreement with that of the Szczepanski et al. study, including those four features to the red of the most intense absorption.

The pentacene cation isolated in Ne shows an intense absorption at 943.9 nm with 3 weaker features at longer wavelengths (see Figure 5D). The absence of a comparable band in Ne and Kr to the 990.3 nm band observed in Ar (see Table 3) indicates that this band is due to the pentacene cation isolated in a different matrix site. Likewise, the observation of the other 3 similar spectral features at longer wavelengths than the most intense absorption in all three matrices suggests that these features are not due to matrix site effects.

In an effort to understand the unusual Franck−Condon envelope of the first absorption band of the pentacene radical cation (Figure 5 and Table 3), we undertook electronic structure calculations. A summary of the results is listed in Table 4. To illustrate these results, we refer to the frontier molecular orbitals of pentacene shown in the upper portion of Figure 6, i.e., the singly occupied MO of the radical cation (SOMO), the orbital just below it (SOMO-1), and the lowest unoccupied MO (LUMO).

TABLE 4: Excitation Energies[a] of the Pentacene Cation

	$X^2B_{3g} \rightarrow 1^2A_u$ (SOMO-1 → SOMO)	$X^2B_{3g} \rightarrow 1^2B_{1u}$ (SOMO → LUMO)
	At Neutral Geometry	
experiment[b]	1.31	
B3LYP	1.49	1.54
TD-B3LYP	1.45	1.40
INDO/S	1.46	1.24
	At Cation Geometry	
experiment[c]	1.31	1.27
B3LYP	1.35	1.34
TD-B3LYP	1.51 (0.229)[d]	1.26 (0.012)[d]
INDO/S	1.53 (0.275)[d]	1.11 (0.023)[d]

[a] In eV. [b] ΔI_{2-1} from photoelectron spectrum in ref 26a. [c] Present work. [d] Oscillator strength for electronic transition.

Exploratory HMO calculations indicated that the transitions involving SOMO-1 → SOMO and SOMO → LUMO molecular orbital transitions and their respective electronic state excitations ($X^2B_{3g} \rightarrow 1^2A_u$) and ($X^2B_{3g} \rightarrow 1^2B_{1u}$) should lie very close in energy (the energy difference between the two excitation amounts to only 0.04 Hückel β-units, which, in the usual spectroscopic parametrization of $1\beta = 3$ eV amounts to 0.12 eV). This semiquantitative expectation was confirmed at the INDO/S−CI level which predicts that, at the geometry of neutral pentacene, the SOMO → LUMO transition occurs at lower energy than the SOMO-1 → SOMO transition (much more so at the equilibrium geometry of the radical cation, cf. last row of Table 4). Furthermore, these calculations indicate that the two excited states in question are well described by single configurations, such that strong nondynamic correlation effects are not to be expected.

The above semiempirical predictions are not in sufficiently good agreement with experiment to permit an unambiguous assignment of the spectra. Since the ground state and the two lowest excited states of the pentacene radical cation are of different symmetry, it is possible to subject them to individual calculations by the B3LYP method which has proven to be quite

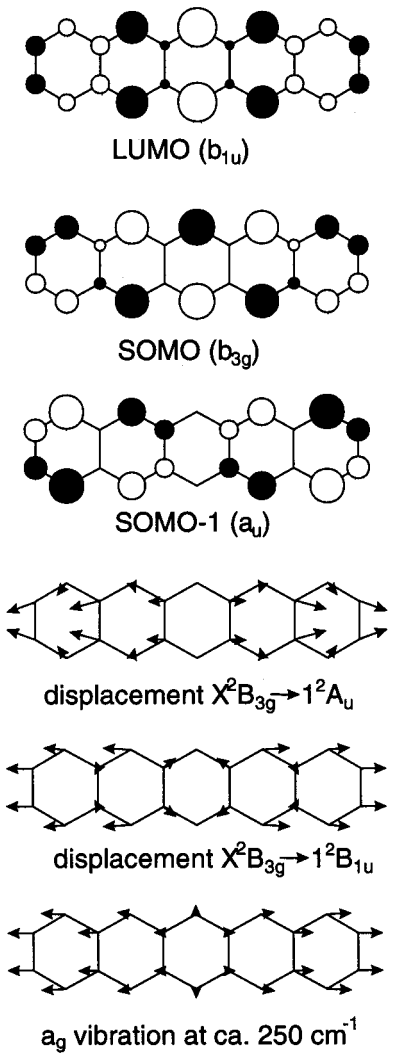

Figure 6. Frontier molecular orbitals and vibrational modes of the pentacene cation.

reliable for excited-state calculations in cases where nondynamic correlation effects are unimportant. In contrast to INDO/S, this method predicts that the 1^2B_{1u} state lies slightly higher than the 1^2A_u state at the geometry of neutral pentacene. However, on going to the equilibrium geometry of the radical cation, the two excited states become nearly degenerate, lying 1.35 eV above the ionic ground state. Both lie close to the intense peak at 943.9 nm (1.31 eV), and to the first band in the spectrum at 979.3 nm (1.27 eV), respectively.

Transition moments cannot be calculated by the normal B3LYP procedure, but they can be determined in the recently introduced time-dependent (TD) variety of DFT (analogous to TD-HF). In this method, the poles of the frequency-dependent polarizability correspond to vertical excitation energies and the pole strengths to oscillator strengths. At the TD-B3LYP level, the $X^2B_{3g} \rightarrow 1^2B_{1u}$ excitation happens to coincide almost exactly with the first, weak band at 979.3 nm (1.27 eV), whereas the $X^2B_{3g} \rightarrow 1^2A_u$ transition appears to be predicted 0.2 eV too high in energy. More importantly, however, the oscillator strength for the $X^2B_{3g} \rightarrow 1^2A_u$ transition is predicted to be more than 10 times higher than that for the $X^2B_{3g} \rightarrow 1^2B_{1u}$ transition, in agreement with INDO/S.

On the basis of the above results, we propose that the "origin" band at 979.3 nm corresponds to $X^2B_{3g} \rightarrow 1^2B_{1u}$ (SOMO $\rightarrow$ LUMO) transition, i.e., to excitation into a state that does not manifest itself in the photoelectron spectrum of pentacene. The strong peak at 943.9 nm is the 0−0 transition of the $X^2B_{3g} \rightarrow 1^2A_u$ (SOMO-1 $\rightarrow$ SOMO) excitation, as originally assigned by Szczepanski et al.[6] Occurrence of excitations into virtual MOs is not unusual in polycyclic aromatic hydrocarbons,[10a,27] but this is the first case of an acene where such an excitation leads to the *lowest* excited state, similar to the case of 2,2-dimethylisoindene radical cation[28] where this was observed for the first time.

TABLE 5: Relaxation Energies and Geometrical Distortions on Excitation of the Pentacene Cation[a]

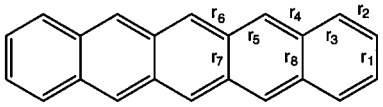

	$X^2B_{3g} \rightarrow 1^2A_u$ (SOMO-1 $\rightarrow$ SOMO)	$X^2B_{3g} \rightarrow 1^2B_{1u}$ (SOMO $\rightarrow$ LUMO)
ΔE_{relax}[b]	-1.47	-3.68
Δr_1	-2.28	-0.10
Δr_2	2.17	0.31
Δr_3	-1.96	0.89
Δr_4	2.79	-1.67
Δr_5	-1.54	2.49
Δr_6	0.97	-0.43
Δr_7	0.09	-1.04
Δr_8	-1.47	0.50

a. From B3LYP/6-31G* calculations; ΔE_{relax} in kcal/mol, Δr_i in pm.
b. Energy difference between vertically formed and geometry optimized states.

Our TD-DFT calculations for the pentacene cation carried out at the neutral pentacene geometry also give us some insight into the assignment for the band of the pentacene cation in Ne at 420.5 nm (Table 3). According to TD-B3LYP, the transition with the largest oscillator strength ($X^2B_{3g} \rightarrow 2^2A_u$, $f = 0.108$) near this observed band is predominantly due to SOMO-2 $\rightarrow$ LUMO excitation. Owing to the excitation into a virtual MO, this state is not accessible directly by ionization of the neutral, and it falls indeed into a region (2.95 eV above the ionic ground state or 9.56 eV above the neutral) where the PE spectrum of pentacene shows a minimum.[26] On the other hand, the 2.78 eV (446.0 nm) energy difference between the fifth and the first band in the PE spectrum corresponds to the $X^2B_{3g} \rightarrow 2^2B_{1u}$ transition which, according to TD-B3LYP, is associated with an oscillator strength that is presumably too weak ($f = 0.022$) for this band to be observed in the optical absorption experiment reported here.

Finally, we would like to address the question of the assignment of the remaining peaks in the spectrum of pentacene radical cation. The bands at 979.3, 955.7, 933.6, and 912.1 nm form a vibrational progression with an interval of ca. 250 cm^{-1}. A similar interval is found between the strong peak at 943.9 nm and a less intense band at 921.5 nm. Vibrational calculations were carried out at the equilibrium geometries of all three states of the pentacene radical cation, and these invariably predict totally symmetric normal modes of very similar shape around 260 cm^{-1}. This a_g mode is depicted at the bottom of Figure 6 which also shows that this vibration coincides very nicely with the displacement vectors on going from the ground state (X^2B_{3g}) to the 1^2B_{1u} or to the 1^2A_u excited state, respectively. The bond length changes that accompany relaxation after vertical excitation from the X^2B_{3g} ground state are listed in Table 5.

Thus, we believe that it is this a_g vibration which is excited on promotion to both excited states. The question remains why only one quantum of vibrational excitation is seen in the 1^2A_u state, whereas three quanta are manifested in the 1^2B_{1u} state. The answer to this question lies in the relaxation energies calculated for the two states (first row of Table 5). That of the 1^2A_u state is calculated to be only 1.47 kcal/mol (515 cm^{-1}), whereas that in the 1^2B_{1u} state is more than twice as high (3.68 kcal/mol, 1290 cm^{-1}). Thus it is clear that the vertical excitation from the X^2B_{3g} ground state of pentacene radical cation occurs into a higher vibrational level in the 1^2B_{1u} state than in the 1^2A_u state, which explains the longer vibrational progression in the former transition.

On the basis of the assignments for the pentacene cation proposed above, and the similarity of the absorption spectrum for the pentacene anion with that of its cation (Figure 5), we tentatively assign the lowest energy absorption at 904.0 nm in Ne to the $X^2B_{1u} \rightarrow 1^2B_{3g}$ (SOMO-1 $\rightarrow$ SOMO) of the pentacene anion. Likewise, we assign the absorption at 872.6 nm in Ne to the $X^2B_{1u} \rightarrow 1^2B_{2g}$ (SOMO $\rightarrow$ LUMO) of the pentacene anion. We associate the vibronic band measured at 883.8 nm in Ne with an a_g vibration which is excited on promotion to the first excited state. A band at a position expected for a $2a_g$ vibronic band for the (SOMO-1 $\rightarrow$ SOMO) transition is not observed and a band at a position expected for an a_g vibronic band for the (SOMO $\rightarrow$ LUMO) transition is also not observed. The spectral region higher in energy than these transitions is obscured by strong absorbances due to the alkali metal and alkali metal−pentacene complexes and prevent the observation of additional spectral features assignable to the isolated pentacene anion.

4. Conclusions

In this study, we have reported the first electronic spectrum of the pentacene anion and cation isolated in a Ne matrix where the perturbation is minimal. Experiments performed with K in the place of Na allow one to disentangle the spectral features of the alkali metal and pentacene complexes from those of the isolated pentacene anions while revealing the degree of isolation of the PAH anions which form upon photolysis of the matrix. The results reported here show that *isolated* pentacene anions can indeed be produced within a rare gas matrix that has been doped with an alkali metal. Use of alkali metal as a matrix dopant can selectively produce molecular anions over molecular cations, allowing for the establishment of molecular charge. Finally, supporting TD-DFT calculations allow new and revised assignments for the pentacene cation and indicate an inversion in energy between the 2 lowest excited-electronic states of the cation as compared to the order in energy of the same states measured in the naphthalene, anthracene, and tetracene cations.[10a,27]

Acknowledgment. The authors thank R. Walker for his invaluable expert assistance in developing the experimental apparatus. T.M.H. also acknowledges the support of the National Research Council in the form of an associateship. This research was supported by NASA's Office of Space Science (Grant No. 344-01-57-41). The work in Fribourg was carried out under Grant No. 2000-053568 of the Swiss National Science Foundation.

Supporting Information Available: Cartesian coordinates and energies of pentacene and its radical cation (in three electronic states), as well as results of TD-B3LYP excited-state calculations on the pentacene radical cation. This material is available free of charge via the Internet at http://pubs.acs.org.

References and Notes

(1) (a) Allamandola, L. J.; Tielens, A. G. G. M.; Barker, J. R. *Astrophys. J. Suppl. Ser.* **1989**, *71*, 733. (b) Puget, J. L.; Léger, A. *Annu. Rev. Astron. Astrophys.* **1989**, *27*, 161. (c) Hudgins, D. M.; Allamandola, L. J. *Astrophys. J. Lett.* **1999**, *513*, L69.

(2) (a) Salama, F.; Bakes, E. L. O.; Allamandola, L. J.; Tielens, A. G. G. *Astrophys. J.* **1996**, *458*, 621. (b) Salama, G. A.; Galazutdinov, G. A.; Krelowski, J.; Allamandola, L. J.; Musaev, F. A. *Astrophys. J.* **1999**, *526*, 265.

(3) (a) Lepp, S.; Dalgarno, A. *Astrophys. J.* **1988**, *335*, 769. (b) Dartois, E.; d'Hendecourt, L. *Astron. Astrophys.* **1997**, *323*, 534. (c) Bakes, E. L. O.; Tielens, A. G. G. M. *Astrophys. J.* **1998**, *499*, 258.

(4) (a) Shida, T.; Iwata, S. *J. Am. Chem. Soc.* **1973**, *95*, 3473. (b) Shida, T. *Electronic Absorption Spectra of Radical Ions*; Elsevier: Amsterdam, 1988.

(5) Henning, T.; Salama, F. *Science* **1998**, *282*, 2204.

(6) Szczepanski, J.; Wehlburg, C.; Vala, M. *Chem. Phys. Lett.* **1995**, *232*, 221.

(7) Crocker, L.; Wang, T.; Kebarle, P. *J. Am. Chem. Soc.* **1993**, *115*, 7818.

(8) Hudgins, D. M.; Allamandola, L. J. *J. Phys. Chem.* **1995**, *99*, 8978.

(9) (a) Kasai, P. H. *Acc. Chem. Res.* **1971**, *4*, 329. (b) Köppe, R.; Kasai, P. H. *J. Phys. Chem.* **1994**, *98*, 12904.

(10) (a) Salama, F.; Allamandola, L. J. *J. Chem. Phys.* **1991**, *94*, 6964. (b) Salama, F.; Joblin, C.; Allamandola, L. J. *J. Chem. Phys.* **1994**, *101*, 10252.

(11) Hudgins, D. M.; Allamandola, L. J. *J. Phys. Chem.* **1995**, *99*, 3033.

(12) Becke, A. D. *J. Chem. Phys.* **1993**, *98*, 5648.

(13) Lee, C.; Yang, W.; Parr, R. G. *Phys. Rev. B* **1988**, *37*, 785.

(14) Stratmann, R. E.; Scuseria, G. E.; Frisch, M. J. *J. Chem. Phys.* **1998**, *109*, 8218.

(15) Frisch, M. J.; Trucks, G. W.; Schlegel, H. B.; Scuseria, G. E.; Robb, M. A.; Cheeseman, J. R.; Zakrzewski, V. G.; Montgomery, J. A.; Stratmann, R. E.; Burant, J. C.; Dapprich, S.; Millam, J. M.; Daniels, D.; Kudin, K. N.; Strain, M. C.; Farkas, O.; Tomasi, J.; Barone, V.; Cossi, M.; Cammi, R.; Mennucci, B.; Pomelli, C.; Adamo, C.; Clifford, S.; Ochterski, J.; Petersson, G. A.; Ayala, P. Y.; Cui, Q.; Morokuma, K.; Malick, D. K.; Rabuck, A. D.; Raghavachari, K.; Foresman, J. B.; Cioslowski, J.; Ortiz, J. V.; Stefanov, B. B.; Liu, G.; Liashenko, A.; Piskorz, P.; Komaromi, I.; Gomperts, R.; Martin, R. L.; Fox, D. J.; Keith, T.; Al-Laham, M. A.; Peng, C. Y.; Nanayakkara, A.; Gonzalez, C.; Challacombe, M.; Gill, P. M. W.; Johnson, B. G.; Chen, W.; Wong, M. W.; Andres, J. L.; Head-Gordon, M.; Replogle, E. S.; Pople, J. A. *Gaussian 98* (Revision A.7); Gaussian, Inc.: Pittsburgh, PA, 1998.

(16) Zerner, M. C.; Ridley, J. E. *Theor. Chim. Acta* **1973**, *32*, 111.

(17) Zerner, M. C. ZINDO, a semiempirical program package; University of Florida, Gainesville, FL 32611.

(18) (a) Balling, L. C.; Havey, M. D.; Dawson, J. F. *J. Chem. Phys.* **1978**, *69*, 1670. (b) Hormes, J.; Karrasch, B. *Chem. Phys.* **1982**, *70*, 29. (c) Balling, L. C.; Wright, J. J. *J. Chem. Phys.* **1984**, *81*, 675. (d) Tam, S.; Fajardo, M. E. *J. Chem. Phys.* **1993**, *99*, 854. (e) Boatz, J. A.; Fajardo, M. E. *J. Chem. Phys.* **1994**, *101*, 3472. (f) Silverman, D. C.; Fajardo, M. E. *J. Chem. Phys.* **1997**, *106*, 8964. (g) Gross, M.; Spiegelmann, F. *J. Chem. Phys.* **1998**, *108*, 4148.

(19) Wright, J. J.; Balling, J. *J. Chem. Phys.* **1980**, *73*, 994.

(20) (a) Coufal, H.; Lüscher, E. *Phys. Lett.* **1974**, *48A*, 445. (b) Coufal, H.; Nagel, U.; Burger, M.; Lüscher, E. *Z. Phys. B* **1976**, *25*, 227. (c) Coufal, H.; Nagel, U.; Lüscher, E. *Ber. Bunsen-Ges. Phys. Chem.* **1978**, *82*, 133. (d) Balling, L. C.; Havey, M. D.; Wright, J. J. *J. Chem. Phys.* **1979**, *70*, 2404. (e) Kuppelmaier, H.; Stöckmann, H.-J.; Steinmetz, A.; Görlach, E.; Ackermann, H. *Phys. Lett.* **1983**, *98A*, 187. (f) Schrimpf, A.; Sulzer, G.; Stöckmann, H.-J.; Ackermann, H. *Phys. Lett.* **1985**, *110A*, 327. (g) Steinmetz, A.; Schrimpf, A.; Stöckmann, H.-J.; Görlach, E.; Dersch, R.; Sulzer, G.; Ackermann, H. *Z. Phys. D* **1987**, *4*, 373. (h) Schrimpf, A.; Sulzer, G.; Stöckmann, H.-J.; Ackermann, H. *Z. Phys. B* **1987**, *67*, 531.

(21) (a) Klevens, H. B.; Platt, J. R. *J. Chem. Phys.* **1949**, *17*, 470. (b) Orlowski, T. E.; Zewail, A. H. *J. Chem. Phys.* **1979**, *70*, 1390.

(22) Heinecke, E.; Hartmann, D.; Müller, R.; Hese, A. *J. Chem. Phys.* **1998**, *109*, 906.

(23) Colangelli, L.; Mennella, V.; Baratta, G. A.; Bussoletti, E.; Strazzulla, G. *Astrophys. J.* **1992**, *396*, 369.

(24) Milligan, D. E.; Jacox, M. E. *J. Chem. Phys.* **1971**, *55*, 3404.

(25) Hudgins, D. M.; Sandford, S. A. *J. Phys. Chem.* **1998**, *102*, 344.

(26) (a) Schmidt, W. *J. Chem. Phys.* **1977**, *66*, 828. (b) Clark, P. A.; Brogli, F.; Heilbronner, E. *Helv. Chim. Acta* **1972**, *55*, 1415.

(27) (a) Andrews, L.; Friedman, R. S.; Kelsall, B. J. *J. Phys. Chem.* **1985**, *89*, 4016. (b) Bally, T. *Chimia* **1994**, *48*, 378.

(28) Forster, P.; Gschwind, R.; Haselbach, E.; Klemm, U.; Wirz, J. *Nouv. J. Chim.* **1980**, *4*, 365.